

Response to Anonymous Referee #2

Holly Still and Christina Hulbe

January 25, 2021

We would like to thank Referee #2 for their helpful feedback on our work. The reviewer's comments are in black and our responses are in blue. Excerpts from the improved manuscript are italicised.

Comments by Reviewer #2

Major comments

Proposed feedback. This comment concerns lines 9-10, 329-337 and 378-384.

(1) I'm not sure I fully understand the proposed feedback: higher backstress from a pinning point is suggested to increase the ice thickness of the ice stream, thereby increasing the driving stress and basal drag which is then reflected by an increased occurrence of sticky spots at the base of the ice stream, making the ice stream less responsive. But to close the loop, the last effect has to feed back on the backstress generated by the ice rumples. How does this work?

It was incorrect to call this a feedback. We will refer to it as a 'connection' between the pinning points and grounded ice instead of as a 'feedback'.

(2) I don't understand how the proposed feedback between pinning points and basal traction of ice streams can be deduced from your experiments. In your inversion you find higher basal friction coefficients in MacIS in comparison to BIS. But if those arise due to the presence of the SCIR cannot be singled out. It could also be that it is the local ice velocity together with the ice thickness field that determines the occurrence of sticky spots in the inverted basal friction coefficient. This is not to say that it might not be possible, but I do not understand how the conclusion 'In the model, the larger basal drag acting on MacIS is itself, via regional changes in driving stress, a consequence of the coupled ice shelf and ice stream response to the SCIR.' can be drawn from the experiments presented in this study.

We agree entirely with this: "*It could also be that it is the local ice velocity together with the ice thickness field that determines the occurrence of sticky spots in the inverted basal friction coefficient.*" What we also assert is that because the thickness and velocity are mechanically connected to the pinning points, they too play a role in setting this property of the bed. What we *have* ignored is the role of the basal hydrology of the ice streams, which may just be different on MacIS than on BIS. This idea arises from the experiment, but

because the model does not simulate hydrology and because the friction coefficient is held fixed, we cannot evaluate it as directly as we would like. This is why we raised the idea in the Discussion. We have edited the Abstract (lines 7-10) to be more clear (we hope)

We find that an ice stream located directly upstream of the pinning points, MacIS, is less responsive to their removal than the obliquely oriented BIS due to zones of locally higher basal drag acting on the main trunk of MacIS. This response is due to the larger basal drag inferred for MacIS, which may itself be a consequence of the coupled ice-shelf and ice-stream response to the pinning points.

In the Discussion and Conclusions sections, we speculate rather than stating that the conclusion can be drawn directly from our experiments:

Line 329: The model experiment presented here suggests a connection between pinning points and grounded ice flow that involves basal traction, and thus basal properties, upstream of the grounding line.

Line 377: Pinning points have been implicated as features that mediate the rate of grounding line retreat, yet their role in conditioning grounded ice flow has received less attention. In the present work, the direct effect of the SCIR on the momentum balance upstream of the grounding line is quantified and an indirect effect, via a connection involving ice stream basal traction, is suggested. This result is obtained by comparison of the relative sensitivity of the adjacent MacIS and BIS to the SCIR.

Basal friction adjustment and ice rise morphology. This comment concerns lines 10-13, 345-346, 386-388 and Figure 3.

(1) In the study, after the inversion procedure, basal friction coefficients of the ice rumples are adjusted in the relaxation simulations. I suppose that this is motivated by large-scale change in the ice rumple morphology when using the inverted basal friction coefficients in the relaxation runs? This would be interesting to extend on, and add the results of the relaxation simulation in Figure 3. Also it would be interesting to see how the overall results of this study would be affected by using the initially inverted basal friction fields.

This was indeed a motivation, along with the poor agreement between the initial inversion result and basal drag inferred using the force budget method. In particular, relatively high basal friction values were assigned to upstream ice rumple nodes and zero values were assigned to the downstream ice rumples (see Fig. 1 at the end of this document). This is contrary to results obtained from the empirical force budget analysis referenced in the manuscript. Because the initially inverted friction coefficient is clearly incorrect, we decided not to pursue further analysis with the incorrect representation, and instead opted to manually tune the friction coefficient to represent all the individual ice rumples in the complex.

Yes, the initially inverted friction coefficient for the SCIR (with no manual adjustment) still reproduces the present-day flow speeds over the rumples, as it must. There is no uniquely correct inverse solution, but beyond that, we are concerned that the inverse approach is unlikely, without some manual intervention, to ever correctly represent these features. At some scale this would not matter but we are able to take advantage of manual mesh refinement to achieve a finer mesh resolution over ice rumples, so it makes sense to ensure that all of the individual ice rumples in the complex (and the associated velocity gradients and resistive stresses) are represented appropriately.

We have added the result of the relaxation simulation with the original, unadjusted friction coefficient to

Fig. 3 in the manuscript (see Fig. 3 in this document for the improved figure).

(2) Overall, a wrong morphology of the ice rumpled after the relaxation simulations does not necessarily imply that the inversion produced wrong basal friction values as implies by statements in lines 10-12 and lines 368-388. It could also be that inconsistencies in the basal or surface mass balance or other factors causes a thinning, thickening, grounding or ungrounding of the ice rumpled during the relaxation period. Don't get me wrong here, I think that your ad-hoc approach to correct the basal friction coefficient is ok. But I think that this should be discussed further and I'd be careful to blame the wrong morphology on the inverted friction coefficients alone. This should be extended on in the discussion.

As noted above, our concern arises in two ways, poor relaxed model morphology *and* poor agreement between our earlier force budget analysis and the initial model inversion.

We do agree that limited knowledge of other boundary conditions could also important. For example, a too large basal melt rate could also lead to ungrounding during relaxation. The basal melting parameterisation used here depends on ice thickness, and therefore the melt rate is largest at the grounding line and decays to zero in the vicinity of the ice rumpled. This is comparable with melt rates inferred by satellite altimetry and works well to reproduce the observed grounding line position as well as the thickness of ice arriving to the area of the rumpled from upstream.

The Supplementary Material includes a section entitled 'Improvements made to the model representation of pinning points'. We have added two paragraphs and figure to the Supplement explaining why we chose to manually adjust the friction coefficient (see Fig. 1 in this document).

The friction coefficient initially inferred for the SCIR (described in Section 2.2) is adjusted to achieve a more realistic ice rumple area and geometry, and to better represent the basal drag inferred by Still et al. (2019). The inversion results in excessively large friction coefficient values (corresponding to $\tau_b > 400$ kPa) inferred for mesh elements on the upstream side of the SCIR complex, and zero values inferred for downstream ice rumple elements (Fig. S2). Landsat 8 imagery indicates that this representation is incorrect. Downstream rumpled provide basal drag and generate surface relief comparable to the upstream rumpled in the complex (implying that basal drag is greater than zero).

To examine sensitivity to basal friction, a range of different friction coefficient values ($\alpha = 0$ to $800 \text{ s}^{1/2} \text{ m}^{-1/2}$) were assigned to the ice rumple nodes before model relaxation. A friction coefficient value that reproduces a relaxed model geometry close to present-day ice velocity and thickness, and that produces a basal drag magnitude similar to the basal drag inferred in a force budget analysis (Still et al., 2019), is used in the model experiments (i.e., $\alpha = 200 \text{ s}^{1/2} \text{ m}^{-1/2}$). The manual adjustment ensured that all of the individual ice rumpled in the complex (and the associated velocity gradients and resistive stresses) were represented in the model geometry (Fig. S2).

(3) Please be more clear: It is stated that 'by extension, any parameter that is affected by the initialization procedure' is represented incorrectly in lines 12-13. What parameters do you mean? Similarly, in line 345 it is stated that 'the present work demonstrates the role of pinning points in parameter selection during model initialization.' Please explain more: What parameters are selected during the initialization procedure that are affected by the pinning points? Which role do the ice rises play? How is this shown in this study?

Lines 12-13: We mean parameters in the governing equations. What we were trying to express here is that incorrect parameter values in one area lead to incorrect parameter values in other areas (by virtue of the minimisation). Perhaps this is a tautology but in any case, it was not clear so we have removed the idea from the abstract. We have also improved lines 12-13 in the abstract:

We also find that inversion of present-day flow and thickness for basal friction and ice softness, without feature-specific adjustment, leads to the incorrect representation of ice rumple morphology and an incorrect boundary condition at the ice base.

The statement in line 345-346 has been improved:

*The present work demonstrates how selection of the **friction coefficient parameter for pinning point nodes** during model initialisation modifies the flow of upstream grounded ice.*

Furthermore, in line 389-390 is stated that ‘The incorrect representation of pinning points also has implications for the inference of model parameters upstream of the grounding line during model initialization.’ My understanding was that you did run the inversion to infer model parameters of basal shear stress and ice softness upstream of the grounding line based on the Bedmap2 geometry in which pinning points should be correctly represented. Or what do you refer to here?

That’s right. We have edited the sentence to:

Although not addressed here, this incorrect representation of pinning points during initialisation also has implications for the inference of the basal shear stress and ice softness parameter upstream of the grounding line.

Formulations. Being more precise with your statements would make it easier for the reader to follow your ideas. For example in line 245 (‘In general, the SCIR act to reduce longitudinal tensile stresses in grounded ice upstream of their location.’): in your next sentence you already mention that this is only partly true depending on the ice softness field used. Here you could directly go to the specific result or you should discuss why the general statement you made before (best supported by literature if it is not textbook knowledge) is actually not true in your experiments. See also comments on lines 293, 309, 319.

We have improved lines 245, 293, 309 and 319, as well as working on clarifying statements in the introduction, results and discussion sections.

We have rewritten lines 245-248 to lead the reader more directly to the point we aim to make. We note that it is generally true that flow obstructions generate compression and our results do not contradict this.

In general, flow obstructions such as pinning points act to reduce longitudinal tensile stresses upstream of their locations and the non-local nature of the momentum balance may allow this affect to extend upstream of the grounding line. In the spatially variable \bar{B}_{inv} case, the SCIR act to decrease longitudinal tensile stresses near the ice stream grounding lines, while in the uniform rate factor \bar{B}_u case, the SCIR have a lesser impact on tensile stresses upstream of the grounding line (Fig. 6c and f). Downstream of the SCIR, the difference between the reference and perturbed models is complicated, with a pattern that depends on both the prescription of \bar{B} and on the geometry of the embayment.

Figure captions. Figure captions should give all relevant information on what is shown in the figure. For

example, sometimes grounding lines are shown, but it is not indicated if this is an observed position or the position obtained in the relaxation simulation or in the respective experiment. In addition, the appropriate grounding lines should be displayed in figures that are interpreted to show changes at the grounding line or upstream (Figs 5,6,7,8,11,12). See also specific comments to the figures.

The appropriate, modelled grounding lines have been added into Figures 5, 6, 7, 8, 9 and 12. These figures are included at the end of this document (Figs. 4-10). Figure 11 in the manuscript has the modelled grounding line displayed in (b).

We have added additional, relevant information to the following figure captions:

Figure 2. Panel (a) shows the inverse rate factor \bar{B}_{inv} in the floating part of the model domain. The value of uniform B_u is shown in the colourbar of panel (a). Panels (b) and (c) focus on MacIS and BIS, showing the friction coefficient α and corresponding basal drag $\tau_b = -\alpha^2 N \mathbf{u}_b$. The grounding line is the observed position from Bindschadler et al. (2011).

Figure 3. Surface morphology and ice velocity for different basal friction coefficient α values assigned to SCIR model nodes. Along-flow surface elevation profiles in panels (a), (b) and (c) demonstrate how selection of the friction coefficient before model relaxation affects ice thickness and surface elevation for three ice rumpled in the SCIR complex...

Figure 4. (a) Modelled ice velocity when $\alpha = 200 \text{ s}^{1/2} \text{ m}^{-1/2}$. (b-d) The difference in ice velocity between the reference model ($\alpha = 200 \text{ s}^{1/2} \text{ m}^{-1/2}$) and alternative relaxed models with varying α values assigned to the SCIR nodes. The grounding line position is the simulated position associated with the differing friction coefficient values.

Figure 5. The gravitational driving stress τ_d acting on the RIS and tributary ice streams with and without the SCIR. In (a-c), the simulation is initialised with \bar{B}_{inv} . In (d-f), the simulation is initialised with \bar{B}_u . In (c) and (f), a positive (negative) change indicates an increase (decrease) in τ_d after removal of the SCIR. The velocity contour lines have an interval of 100 ma^{-1} . Grounding line positions in (a) and (d) are obtained from the \bar{B}_{inv} and \bar{B}_u reference models (with SCIR). Grounding line positions in (b) and (e) are obtained from the \bar{B}_{inv} and \bar{B}_u perturbed models (without SCIR).

Figure 9: The total difference in ice speed between the steady-state, \bar{B}_{inv} reference model (with SCIR) and the perturbed model (without SCIR) at various model timesteps following removal of the SCIR. (a) is the instantaneous response and (b-c) demonstrate the longer timescale adjustment of the ice-shelf and ice-stream system. Positive values indicate faster flow and negative values indicate slower flow. By a timestep of 150 years, the model has reached a new steady-state. The velocity contour lines have an interval of 100 ma^{-1} .

Figure 10. Model shear strain rates near the SCIR for (a) and (b) spatially variable ice properties (\bar{B}_{inv} model) versus (c) and (d) uniform ice properties (\bar{B}_u model). Grounding line positions are obtained from the reference and perturbed models.

Figure 11. (a) The total change in ice thickness 150 years after removal of the SCIR. Red indicates thinner ice and blue indicates thicker ice without the ice rumpled. (b) Retreat of a section of the simulated MacIS grounding line (\bar{B}_{inv} case) following removal of the SCIR plotted on the subglacial bed elevation (Fretwell et al., 2013).

Further comments

Line 9-10: see major comment.

Please refer to our response to the major comment.

Line 10-13: see major comment.

Please refer to our response to the major comment.

Line 15: ‘transient’ changes in ice shelf geometry in contrast to ‘persistent’ changes in ice streams. I’m not sure I understand this statement as the changes in ice thickness and speed that you present in Figures 9 and 11 are visible in both, the ice shelf and the ice streams.

MacAyeal and Bindschadler Ice Streams speed up in response to removal of the SCIR, with no slow-down after the maximum velocity has been reached (60-70 years after pinning point removal). In contrast, some regions of the eastern Ross Ice Shelf initially exhibit an increase in flow speeds in response to SCIR removal, then the ice speed decreases as the ice shelf adjusts to a new steady state. This is what we meant by ‘persistent’ and ‘transient’. This could be described more clearly and we have changed it to:

Viewed from the perspective of change detection, we find that the ice shelf undergoes an adjustment to a new steady-state that involves an initial increase in ice speeds across the eastern ice shelf, followed by decaying flow speeds, as mass flux reduces thickness gradients in some areas and increases thickness gradients in others. Changes to ice-stream flow speeds persist without further adjustment, even without sustained grounding-line retreat.

Figure 1: Add Echelmeyer Ice Stream as you are referring to it later on.

We first mention Echelmeyer Ice Stream when describing Fig. 9 so we have added the label to the maps in this figure.

Line 21: Another interesting study analyzing this is done by Pegler in 2018 (‘Marine ice sheet dynamics: the impacts of ice-shelf buttressing’).

We will add the reference to Pegler (2018) to Line 21.

An ice shelf laterally confined within an embayment experiences reduced longitudinal tensile stress (and stretching) relative to an unconfined ice shelf due to lateral shearing where the ice flows past coastal features and islands (Sanderson, 1979; Haseloff and Sergienko, 2018; Pegler, 2018).

Lines 24 and 61: A bit of care with the wording should be taken here. The term ‘flow-buttressing’ has been used previously in Furst et al. It calculates the buttressing parameter by selecting the ice flow direction as a normal direction. However, the ice flow direction can be very different to the normal direction at the grounding line which is used in Gudmundsson 2013 to calculate a buttressing parameter.

This is an excellent point. We conducted an analysis in the style of Furst et al. but did not include it here (read Still’s thesis!). Line 24 has been changed to be correctly inclusive:

Altogether, the rate of mass flux is moderated in an effect commonly referred to as the ‘flow buttressing’ exerted on upstream grounded ice by the ice shelf (Dupont and Alley, 2005, 2006; Gudmundsson, 2013; Furst

et al., 2016).

Lines 65 and 118: ‘models’ → ‘model configurations’ as ISSM is only one model?

Changed as suggested.

Section 2.2: How is the basal friction parameter set in regions that are not grounded during the inversion but that ground during the transient forward simulations? How is basal friction treated in elements along the grounding lines?

Basal friction at the grounding line (for partially grounded model elements) is treated using the sub-element parameterisation (‘SEP2’) of Seroussi *et al.* (2014). Here, the friction coefficient for a partially grounded element is scaled to the area of grounded ice within an element (e.g., Gladstone *et al.*, 2010; Seroussi *et al.*, 2014) (the friction coefficient is defined at each mesh node). The friction coefficient for ice that grounds during transient simulations is specified according to the original inferred basal friction map (i.e., zero for floating ice). We do not adjust the friction coefficient downstream of the grounding line to a non-zero value (in case of grounding line advance) because the friction coefficient immediately upstream of the MacAyeal and Bindshadler Ice Stream grounding lines is already equal to zero (ice streams are low basal traction environments). It’s also worth noting that no floating ice runs aground in the perturbed model simulations. We have added a statement to Section 2.1 ‘Ice Sheet model’.

Both grounding-line migration and the representation of basal friction for partially floating elements (as the grounding line migrates) are treated using the sub-element parameterisation scheme (‘SEP2’) of Seroussi et al. (2014).

Line 163: Why 150 years?

The rates of change in model ice volume, thickness, and speed were tracked to identify when a ~steady state had been achieved. 150 years is when the rates of change reach 0.001%.

We have clarified this in the text (line 160):

The steady-state reference model is perturbed by excavating the bathymetry beneath the SCIR to prevent mechanical contact between the ice and seafloor, and stepped forward for 150 years with a timestep of 1 year. By 150 years, the rate of change in ice shelf volume is 0.001%, indicating that the model has reached a new steady-state.

Figure 2: It would be helpful to add here that also B_u is shown in the colorbar of panel (a).

Changed as suggested.

Figure 3: It would be helpful to have (a) also the surface and velocity profile obtained with the inverted basal friction coefficient in the panels and (b) the magnitude of the optimized coefficient (e.g., averages along the lines). In addition, in panel (d) is the grey box showing the grounded regions in Bedmap2?

We have added surface elevation and velocity profiles obtained with the original inverted basal friction to Figure 3 as dotted line (see Fig. 3 at the end of this document).

A figure demonstrating the magnitude of the optimised friction coefficient has been added to the supplementary material following suggestion (b) above (Fig. 2 in this document).

The grey boxes in (a) to (d) show grounded sections in the steady-state model geometry. Panel (e) shows the geometry of the steady-state reference model. In the figure caption we state that: *Grey shaded boxes indicate model nodes where the ice shelf is grounded.*

Line 149: Is the same time stepping also applied in the perturbation experiments? If yes, how is the snapshot after 1 year shown in Figure 9(a) obtained?

Good point. We've improved the relevant sentence in Section 2.3 Experiment design:

The steady-state reference model is perturbed by excavating the bathymetry beneath the SCIR to prevent mechanical contact between the ice and seafloor, and stepped forward for 150 years with a timestep of 1 year.

Line 175: How is the morphology for the different friction coefficients obtained? I suppose that the 1000 years relaxation was run with different basal friction coefficients for the ice rumples?

This is correct. We have modified this sentence (Line 175):

*The friction coefficient assigned to ice rundle nodes is manually adjusted **before model relaxation** to reproduce both observed ice flow and rundle morphology (Fig. 3).*

And we've modified the figure caption:

Fig. 3. Surface morphology and ice velocity for different basal friction coefficient α values assigned to SCIR model nodes. Along-flow surface elevation profiles in panels (a), (b) and (c) demonstrate how selection of the friction coefficient before model relaxation affects ice thickness and surface elevation for three ice rumples in the SCIR complex...

Line 184: How does the optimized value compare to this value (see also comment on Figure 3)?

The optimized value varies spatially and ranges from 0 to $490 \text{ s}^{1/2} \text{ m}^{-1/2}$. The optimized values does not capture the spatial extent of the ice rumples and thus we only focus on the simulations with manual tuning of the friction coefficient for the ice rumples. A figure has been added to the Supplementary Material (see Fig. 1 in this document).

Line 192: Fig S2.

Corrected.

Figure 4: Is this an instantaneous velocity difference or a difference obtained after running the relaxation for 1000 years with the corresponding basal friction coefficient? What grounding line position is shown? If it is not shown here, it would be helpful to show the final grounding line positions after the relaxation runs to see how the ice rundle geometry is affected by the adjustment.

The figures show the difference between two steady states, with differing friction coefficients manually assigned to the SCIR (not the instantaneous difference). The grounding line position is the present-day position rather than the modelled position. Ice rundle grounded area remains unchanged in the friction

coefficient $\alpha = 0, 200, 400, 600$ models because we excavated the bathymetry around the rumples to prevent an increase in ice rundle area. Ungrounding of downstream rumples occurs in the $\alpha = 0$ model.

We have added the final grounding line positions (after relaxation) to the figure and improved the caption:

(a) Modelled ice velocity when $\alpha = 200 \text{ s}^{1/2} \text{ m}^{-1/2}$. (b-d) The difference in ice velocity between the reference model ($\alpha = 200 \text{ s}^{1/2} \text{ m}^{-1/2}$) and alternative relaxed models with varying α values assigned to the SCIR nodes. The grounding line position is the simulated position associated with the differing friction coefficient values.

Section 3.2: What is your main finding or conclusion from this comparison in relation with the later chapters? I think that it would help for the following chapters to analyze the difference and similarities between the results in light of the robustness of the results.

This section focuses on the differences between the simulations with variable and uniform \bar{B} .

The broad conclusions would be the same with either \bar{B}_u or \bar{B}_{inv} , which is indeed interesting. However, there are differences over limited spatial extents that might be important for some applications, for example, how changes in pinning points might drive changes in crevasse mechanics.

\bar{B}_{inv} is important for routing of ice around rumples (i.e., weaker ice in shear margins is represented, thus facilitating ice flow around an obstacle). The differences demonstrate that the inferred pattern of \bar{B} near a pinning point does impact the pinning point contribution to flow resistance.

These concerns are raised in the manuscript.

Line 221-222: This statement seems to be true for the largest of the ice rumples but not for the smaller, second-largest one to the left?

Thanks for this comment. We know what is going on here but did not describe it. Pinning points lead to a smaller thickness gradient and surface slope upstream of their location, so when they are removed, the gradients and driving stress can increase upstream. Downstream, the opposite happens. This has been explained in the manuscript. We have modified Lines 221-223 to be more specific about where changes in τ_d are occurring:

Pinning points generate locally large thickness gradients that in turn support the relatively high τ_d near the largest ice rundle (Fig. 1). This geometry is required to maintain mass flux past the obstacles. Upstream of the SCIR, relatively thicker ice with a lower surface slope leads to lower driving stresses in comparison to the configuration without the SCIR.

Line 222-226: Since the figure does not show a grounding line position, it is hard to say, but from a rough estimate it does not look like driving stress along the grounding lines of the glaciers main trunks change significantly? It would be helpful if you (1) add the grounding lines in the Figure and (2) add the driving stress changes in Table 3. In addition, do you know what the blue spots in MacIS in the B_u case are? Could they be numerical artifacts in individual mesh elements?

We have added the grounding lines to the figure (Fig. 4 in this document) and clarified the text, providing a sense of scale:

In the perturbed model, thinning upstream of the former SCIR results in a larger thickness gradient and locally larger driving stresses immediately downstream of the grounding lines of MacIS and BIS, and in some locations, the locally larger τ_d (on the order of 10 kPa) and mass flux drive grounding line retreat (Section 3.4).

The flux gates used for Table 3 are not in locations that would demonstrate what is described here and we are not sure how to make them useful to this cause.

The original paragraph considered only ice on the floating side of the grounding line. We have added a short paragraph describing the situation upstream of the grounding line:

The SCIR may also affect τ_d upstream of the grounding line. Patches of relatively large decreases in the driving stress (blue patches in Fig. 5f) coincide with local lows in the bed elevation where thinner ice goes afloat in the perturbed model. Elsewhere, the differences between the two simulations are small, <5 kPa. The model does not simulate basal hydrology and α is held fixed, both of which may be variable and contribute to dynamic change in the driving stress.

Line 227: How do you conclude that changes in flow buttressing are equal in both cases?

We were able to make this conclusion because we computed the along flow and maximum buttressing numbers of Fürst et al. (2016) using our model output (B_{inv} and B_u , reference and perturbed model). While interesting, it did not add any additional insight into pinning point behaviour and we included only the force budget approach in the manuscript. We have removed this statement.

Line 235: Is this pattern consistent with the location of sticky spots and topographic features?

The relevant sentence: *Along the main trunk of MacIS, peaks in $-\bar{R}_{ll}$ form a ‘rib-like’ pattern characteristic of ice flow over sticky spots and an uneven subglacial bed topography (Fig. 6).*

Peaks in $-\bar{R}_{ll}$ are somewhat consistent with topographic lows in the Bedmap 2 subglacial topography. Peaks in the across-flow compressive stress $-\bar{R}_{tt}$ have much better correspondence with topographic lows in the Bedmap2 subglacial topography and the location of sticky spots (i.e., locally high friction coefficient values). A ridge that is visible in the surface topography (in the MODIS MOA) is also captured by $-\bar{R}_{tt}$.

The main point we aim to make is that this pattern is consistent with other studies:

Line 285 in the original manuscript: *Model initialisation results in a greater density of sticky spots on MacIS than on BIS, a result that is consistent with other inversions of observed velocities (Joughin et al., 2004; Sergienko et al., 2008), observations of ice stream surface morphology and textures (Stephenson and Bindshadler, 1990; Bindshadler and Scambos, 1991), and seismic surveys (Anandkrishnan and Alley, 1994; Luthra et al., 2016).*

Line 244: Not sure I understand this statement, Figure 8 shows particularly high lateral shear stress in this area?

We have rewritten Line 244:

At this location, basal and lateral shear stresses make a lesser contribution to the force balance. The $+\bar{R}_{ll}$ pattern is stronger in the B_{inv} case (Fig. 7).

Line 244: ‘exaggerated’ → ‘stronger’? Since B_{inv} is obtained through inversion, I would expect the velocity and ice softness field to be closer to present-day than for the ad-hoc assumption of constant B_u . Thus, I would think of B_{inv} as the reference simulation and B_u as a test case to support robustness.

Corrected as suggested.

Line 247: Fig.6 → Fig.7.

Thanks, we corrected this.

Line 272: ‘increase divergence downstream of their location’ - this seems to depend on the ice softness and there is a large spot of decreased divergence (red) directly next to the rumples (on their western side) and downstream?

Agreed. We have improved the description of Fig. S7, beginning Line 272:

In general, the SCIR reduce flow divergence in the region between Roosevelt Island, and the MacIS and BIS grounding line, with the pattern of R_{tt} depending on the selection of B_{inv} or B_u (Fig. S7). Localised increases in divergence originate from individual ice rumples in the SCIR complex as ice flows over each obstacle. The SCIR also increase convergence near the outlet of Echelmeyer Ice Stream (Fig. S6), but to the south, the SCIR create a diverging geometry and transverse tensile stresses that are locally larger in comparison to the perturbed model without the ice rumples.

Section 3.3.5: Maybe move this earlier so that you define ‘sticky spots’ before you discuss them in Section 3.3.2.

Good point. Section 3.3.5 (Basal drag) now follows Section 3.3.1 (The driving stress).

Figure 9: which case is shown here, B_{inv} or B_u ?

We have added this to the figure caption.

Line 285-286: It is really hard to tell from Figure 9 in which ice stream the speed increases more after 150 years. Would maybe be helpful to point to Table 3 here and add also absolute and relative speed changes along the glaciers grounding lines (and maybe move figures to the SI). In addition, it would be interesting to have an estimate of how far speed changes extend inland for both glaciers.

Excellent, thank you. We have added a reference to Table 3 and a figure to the Supplementary Material to demonstrate the greater increase in flow speed exhibited by Bindschadler Ice Stream (see Figure 2 in this document).

We have added an estimate of how far speed changes extend inland (after line 286):

Similarly, differences in ice stream flow speeds with and without the SCIR extend further inland for BIS than for MacIS. A total speed change of $\geq 5 \text{ m a}^{-1}$ extends 280 km upstream of the BIS grounding line, and 230 km upstream of the MacIS grounding line.

Section 3.4: I suggest to move this section before the changes in stresses are discussed to give the reader first an idea of how thickness, grounding line position and velocities change which then also makes it easier to interpret them with respect to changes in stresses.

The aim of the work was to quantify the role that the SCIR play in the momentum budget of the ice shelf and ice stream system. Thickness and velocity are consequences of this. We think that the *why* of ice sheet change is sometimes obscured or devalued relative to the *what* and the intent of organising the sections with the resistive stresses first was to insist that the *why* is important.

Line 293: Please be more precise here. How does this feedback work?

We changed the word ‘feedback’ to ‘connection’. More details are elsewhere in this response.

Line 296-303: That you find an immediate slow-down upstream of the ice rumples is surprising and interesting to me. I think that your explanation that the initial slow will be reversed once the ice thins in the location of the ice rumples could be supported more: you could do an additional, simple experiment in which you do not only remove the ice rumples in the topography but also thin the ice at their former location so that the perturbed ice shelf is flatter (i.e., using the thickness distribution after 5 years) and then compare the instantaneous response. If the response is similar to your current 5 year response, then the initial response can most likely be linked to the initial thickness distribution in your perturbation experiment.

We agree that this is interesting. Our “explanation” is what we observe in the model simulation, as described in the manuscript. If we understand the comment correctly, the relaxation accomplishes what the reviewer is after without manual manipulation of the ice thickness.

Line 309-311: Be more specific here, what do you mean with ‘the fundamental mechanisms are generic’?

We have improved lines 309-311:

The magnitude and spatial pattern of the transient response is specific to the experimental design that intended to quantify the SCIR contribution to the mechanics of the RIS, rather than to investigate externally-forced change, such as pinning point modification due to basal melting. The fundamental mechanisms investigated here (i.e., the redistribution of stresses and the longer-timescale adjustment of ice flow and thickness), apply regardless of forcing.

Line 310 ‘mechanics and dynamics’ → ‘mechanics of Ross Ice Shelf’?

Changed as suggested.

Line 319-320: Be more precise here. A redistribution of mass from where to where? Is it large or small? And how do the pinning points affect the efficiency by pinning points?

We have added a reference to the figures that demonstrate how mass is redistributed across the RIS in response to the pinning points and changed the text.

Altogether, the pinning points cause a redistribution of mass (Figs. 10a and 11a) and only a small increase in the total ice volume stored in the eastern RIS.

Discussion: Discussion should be extended to include also a discussion of the model choices done here (e.g., sliding law), potential drawbacks and limitations of the methodology (e.g., assuming that present-day Ross Ice Shelf and the Siple Coast Ice Streams are in steady-state).

We have added the following two paragraphs to the Discussion section:

The choice of friction law and its coefficients determine ice stream flow speeds and mass flux across the grounding line. The Budd-type friction law (Budd et al., 1979) used here is a common choice in ISSM applications, where it has been found to improve model stability and representation of grounding line migration (Seroussi and Morlighem, 2018). The grounding line is more sensitive to change than would be the case for other possible friction laws (Tsai et al., 2015; Brondex et al., 2017; Joughin et al., 2019).

The inferred basal friction coefficient α encapsulates the mechanical and thermal properties of the ice/bed interface in a single, spatially varying, parameter. Individual physical processes that control basal sliding (e.g., till deformability, presence of subglacial meltwater, bedrock bumps) are therefore hidden within the friction coefficient distribution. Without additional parameterisations to account for change in these processes over time, α is held fixed. Given the apparent dynamical connections between pinning points and basal traction on grounded ice (identified here and by Nias et al. (2016)), improved representation of sliding and of the processes responsible for basal friction are likely to lead to new insights into the behaviour of the coupled system.

We have revised the description of the experiment design, two regimes with and without the SCIR, to be more clear about the motivation and about the “assumption” of steady state. We need a steady state as a reference against which to most easily compare the perturbed model. Where the steady state assumption causes a problem is the inference of parameter values during initialisation – the inversion assumes a steady state *and* we go on to hold these values fixed. We are not alone in facing this dilemma and we discussed implications but these are distributed through the Discussion, where they are relevant to specific issues, rather than in a stand-alone section.

For example, in the Discussion, we state:

Line 360: From an ice dynamics point of view, this result is obtained at least in part because softer ice at the margin limits the transfer of resistive stresses generated by coastal features to the wider ice shelf. Because \bar{B} is a fixed property of model elements set during initialisation, this particular pinning-point effect persists after the pinning point is lost, and in turn, facilitates retreat.

Line 364: There may be unintended consequences of fixed, constant \bar{B} as relatively low total strain can change crystallographic preferred orientation, and thus \bar{B} , within an ice shelf or ice stream (Duval and Castelnau, 1995; Lutz et al., 2020; Jordan et al., 2020).

Line 329-337: I’m not sure I understand this feedback, see also the main comment.

We changed the word ‘feedback’ to ‘connection’. More details are elsewhere in this response.

Line 335-338: This sentence could be misunderstood to indicate that the studies of (van der Wel et al., 2013; Hoffman and Price, 2014) investigate a physical coupling between pinning points and ice stream basal properties (none of the studies includes dynamic ice shelves).

Indeed. These are interesting ideas that arose when *we* were re-reading those papers, after having conducted the experiments reported here. The simplest thing is to remove the references in line 336.

The lower basal traction explains the greater responsiveness of BIS to the SCIR in the model simulations. In the real system, such a coupling could involve stress-driven changes in basal water flow and till properties

that in turn affect basal friction.

Line 338: Looking into Table 3, the relative mass flux increases following SCIR removal of MacIS and BIS seem quite close when comparing it to other ice streams listed. I agree that it is interesting that BIS shows a similar and slightly higher response than MacIS which is located more directly upstream of the SCIR, but calling it a ‘contrast’ is maybe a bit too much.

We will replace ‘contrast’ with ‘difference’. *The difference between MacIS and BIS sensitivity to the SCIR highlights...*

Lines 345-346: See major comment.

We should have stated that we were referring specifically to the friction coefficient inferred during model initialisation. Line 345-346 has been changed to:

The present work demonstrates how selection of the friction coefficient parameter for pinning point nodes during model initialisation modifies the behaviour of the wider RIS.

Conclusions: in this section it would be great if you could put your findings into a broader context, e.g., discussing the vulnerability of the SCIR in a changing climate and the implications of your work in this context.

We have added a paragraph to the discussion that considers the importance of the SCIR to long-term ice-shelf stability.

The magnitude of the flow resistance currently provided by the SCIR is of the same order of magnitude as the flow resistance provided by the larger and more well-grounded Roosevelt, Crary and Steershead Ice Rises (Still et al., 2019). This finding alone does not reveal how important the SCIR are to RIS stability. If an unstable ice shelf configuration is required for irreversible grounding line retreat (Weertman, 1974; Schoof, 2007), then the simulations imply that the SCIR are unimportant to stability (SCIR removal results in a transition to a new steady-state), despite the relatively large flow resistance they provide. This is due to a regional redistribution of ice thickness and resistive stresses. The redistribution, which itself depends on embayment geometry, moderates the sensitivity of the coupled ice sheet–ice shelf system to the ice rumples. Similar redistributions should be expected for changes to other, individual pinning points. If stability is associated with crevasse and rift formation (Bassis and Ma, 2015; Borstad et al., 2017; Lai et al., 2020), the SCIR generate shear and tensile stresses that form crevasses and therefore the removal of pinning points may be expected to improve stability, although changes to shear stresses elsewhere may promote crevasse and rift formation in those locations. If stability is associated with ice shelf thickness (Gudmundsson et al., 2019), the SCIR cause a regional redistribution of mass with a net effect of about a 1% change in ice shelf mass, implying very little impact on long-term stability.

Line 387-388: This could be misunderstood to mean that you did apply the feature-specific tuning during the inversion and not after the inversion. The second part of that sentence could be misinterpreted to state that the ice rumple morphology influences the overall results of this study, but this is not shown, as the results from Figs 5 to 12 are all done using the same basal friction coefficient for the ice rumples.

We agree that this is unclear and we have expanded upon this sentence:

Naive inversion for the friction coefficient with no further evaluation or adjustment, where appropriate data are available, may lead to the incorrect representation of pinning point morphology, ice velocity, and the upstream flow resistance provided by pinning points. Over-simplifying or exaggerating the relative importance of pinning points in a model may lead to over- and under-estimates of the role of pinning points in the ice-shelf and grounding-line response to climate forcing.

Line 388-390: see major comment.

Please refer to our response to the major comment.

Figure 10: Please also add the formerly grounded region in background of panels a and b.

The formerly grounded region is indicated in Figure 10c. The ‘distance along flowline’ labels along the x -axis are consistent between subfigures.

Fig S5: What is shown in the background of the figure?

The background is the ice thickness and we have added the missing colorbar. The content of this figure is now included in Fig. 1 in the manuscript (see Fig. 11 in this document).

Additional figures for the Supplement

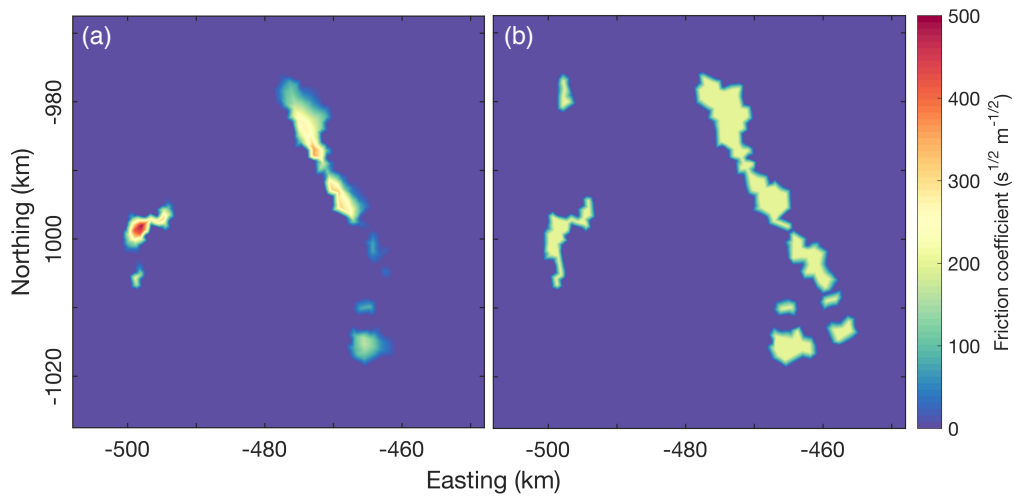


Figure 1: (a) The initial friction coefficient resulting from the inversion with no manual adjustment and (b) is the friction coefficient adjusted to represent the basal drag computed by [Still et al. \(2019\)](#).

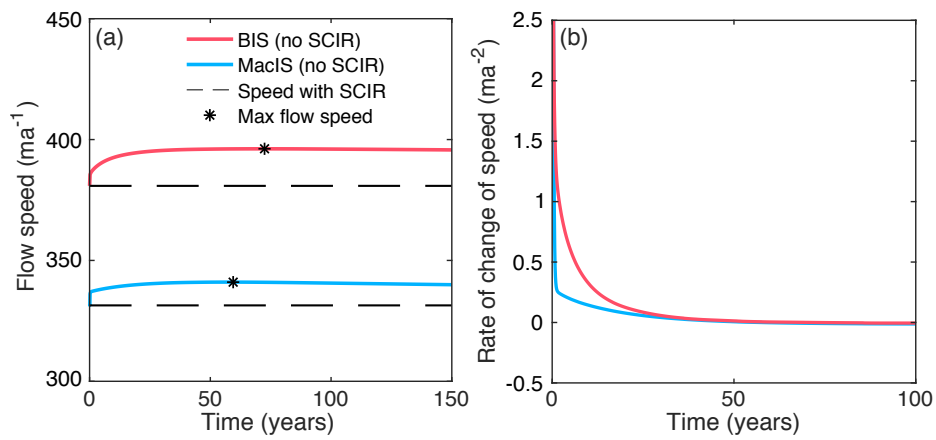


Figure 2: Comparison between the responses of MacIS and BIS to removal of the SCIR. (a) Ice stream flow speeds and (b) the change in flow speed computed at each timestep are computed as spatial averages across the main ice stream trunks. The ‘time’ variable refers to the number of years after removal of the SCIR.

Modified figures

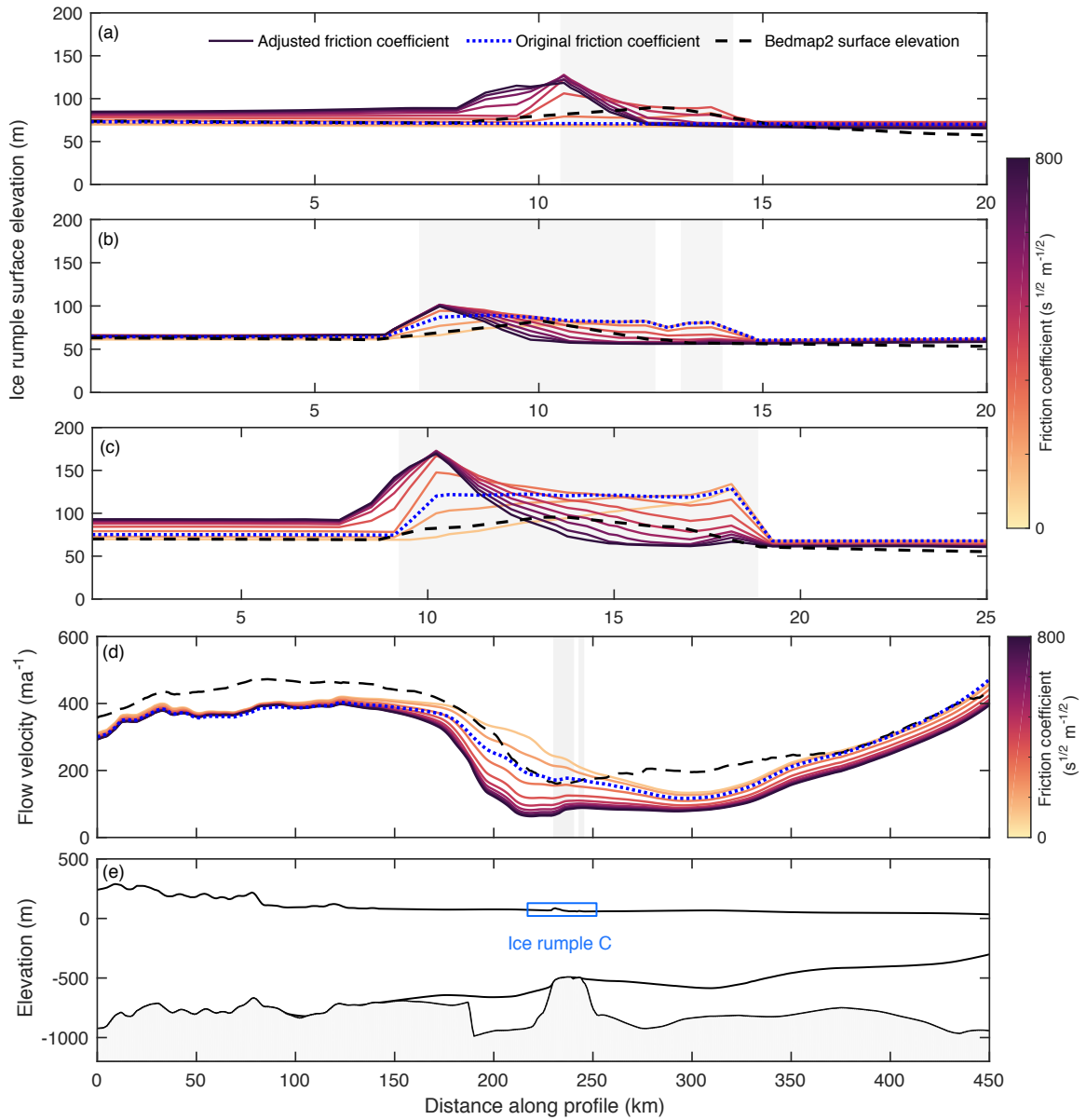


Figure 3: Surface morphology and ice velocity for different basal friction coefficient α values assigned to SCIR model nodes. Along-flow surface elevation profiles in panels (a), (b) and (c) demonstrate how selection of the friction coefficient before model relaxation affects ice thickness and surface elevation for three ice rumples in the SCIR complex (ice rumples A, B and C, respectively, see Fig. 1b for their location). Grey shaded boxes indicate model nodes where the ice shelf is grounded. Panel (d) demonstrates how selection of the friction coefficient affects the velocity magnitude. The profile in (d) represents a single pathway that begins 150 km upstream of the MacIS grounding line, intersects the SCIR rumple C, and ends at the shelf front. Panel (e) shows ice thickness and the underlying seafloor along this pathway in the reference model. The locations of the profiles in (a) to (e) are mapped in Fig. 1b.

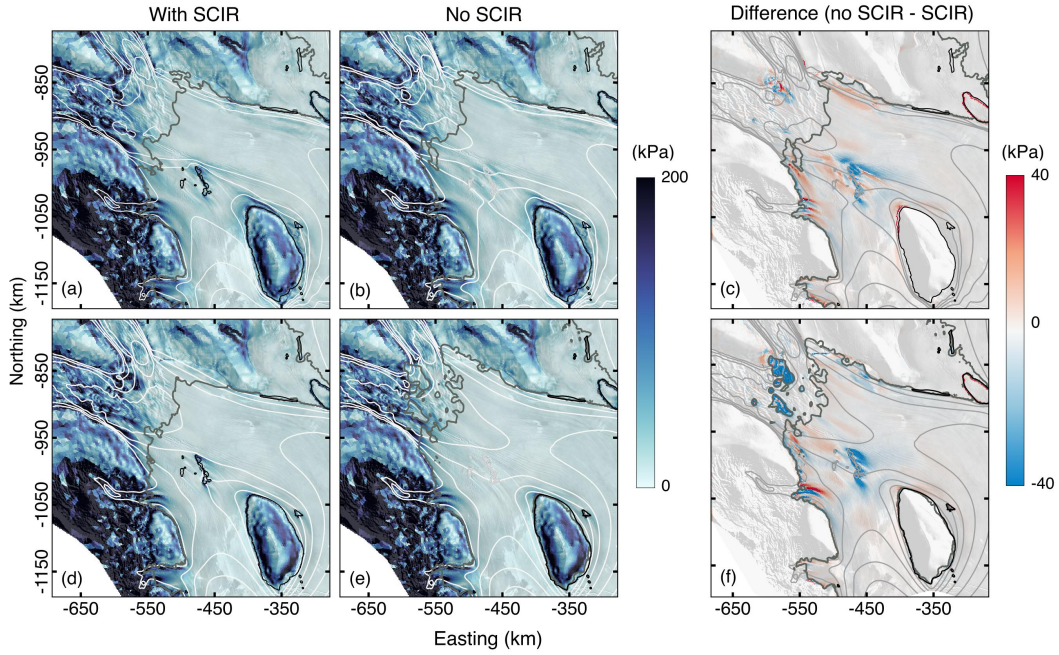


Figure 4: The gravitational driving stress τ_d acting on the RIS and tributary ice streams with and without the SCIR. In (a-c), the simulation is initialised with \bar{B}_{inv} . In (d-f), the simulation is initialised with \bar{B}_u . In (c) and (f), a positive (negative) change indicates an increase (decrease) in τ_d after removal of the SCIR. The velocity contour lines have an interval of 100 m a^{-1} . Grounding line positions in (a) and (d) are obtained from the \bar{B}_{inv} and \bar{B}_u reference models (with SCIR). Grounding line positions in (b) and (e) are obtained from the \bar{B}_{inv} and \bar{B}_u perturbed models (without SCIR).

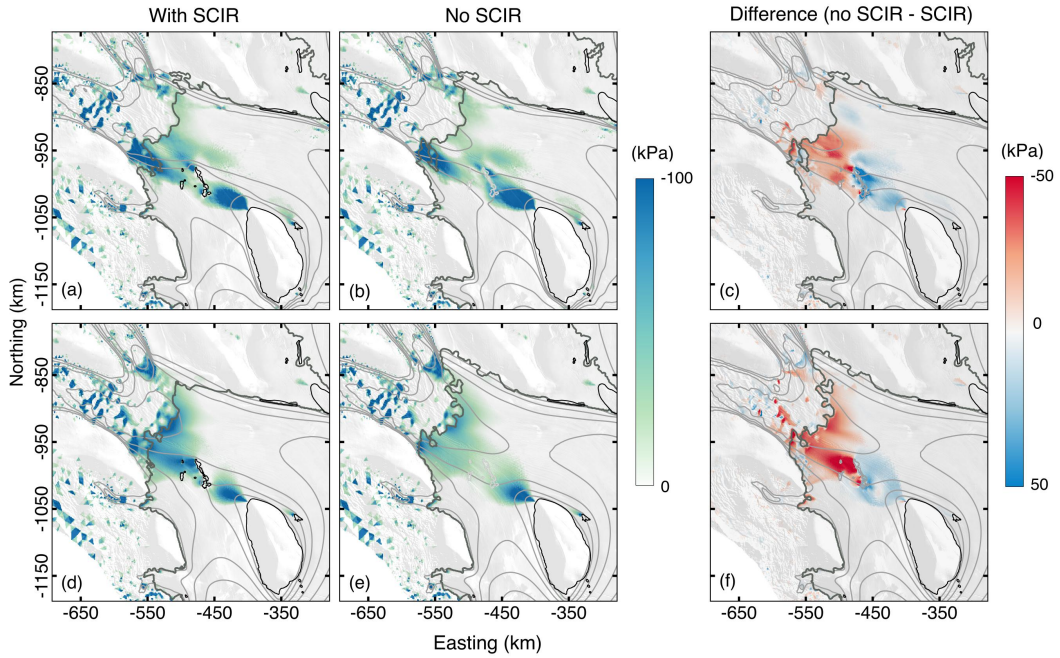


Figure 5: The longitudinal compressive stress $-\bar{R}_l$ acting on the RIS and tributary ice streams with and without the SCIR. In (a-c), the simulation is initialised with \bar{B}_{inv} . In (d-f), the simulation is initialised with \bar{B}_u .

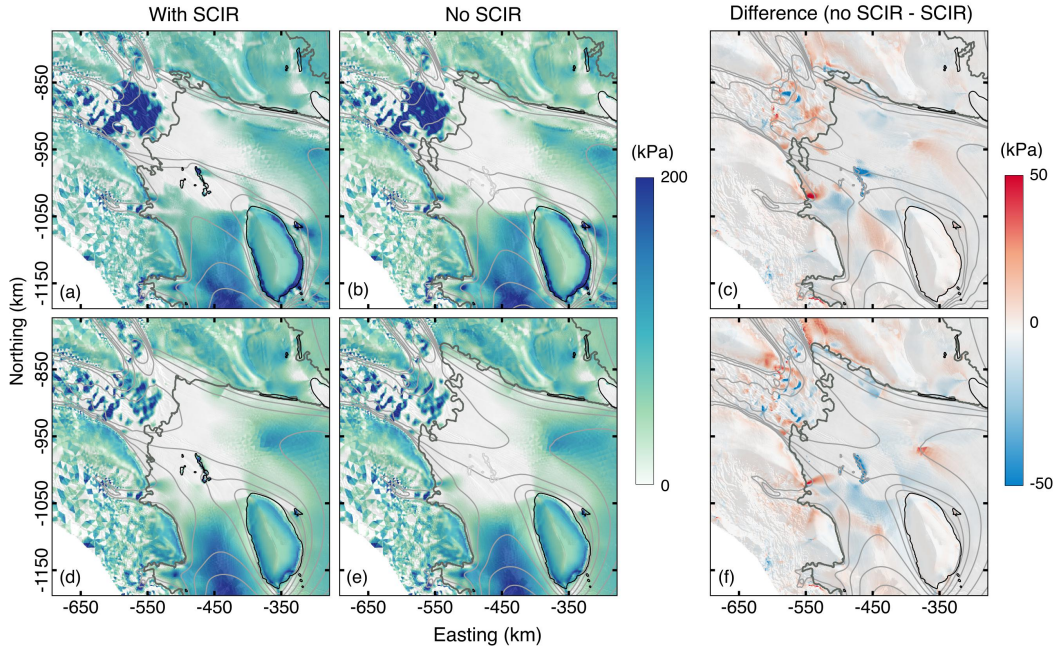


Figure 6: The longitudinal tensile stress $+\bar{R}_{||}$ acting on the RIS and tributary ice streams with and without the SCIR. In (a-c), the simulation is initialised with \bar{B}_{inv} . In (d-f), the simulation is initialised with \bar{B}_u . In (a) and (b), the unusually high $+\bar{R}_{||}$ values at the outlet of MacIS and BIS are due to relatively high B_{inv} values inferred during model initialisation.

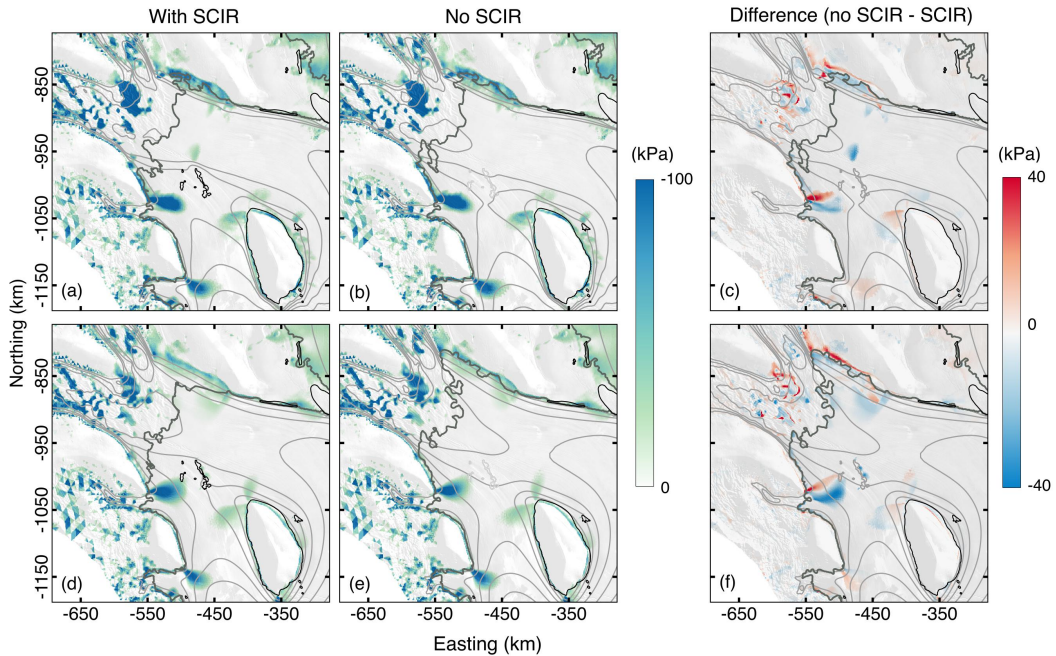


Figure 7: The transverse stress $-\bar{R}_{tt}$ (flow convergence) acting on the RIS and tributary ice streams with and without the SCIR. In (a-c), the simulation is initialised with \bar{B}_{inv} . In (d-f), the simulation is initialised with \bar{B}_u . In (c) and (f), positive (negative) values indicate an increase (decrease) in flow convergence when the SCIR are removed.

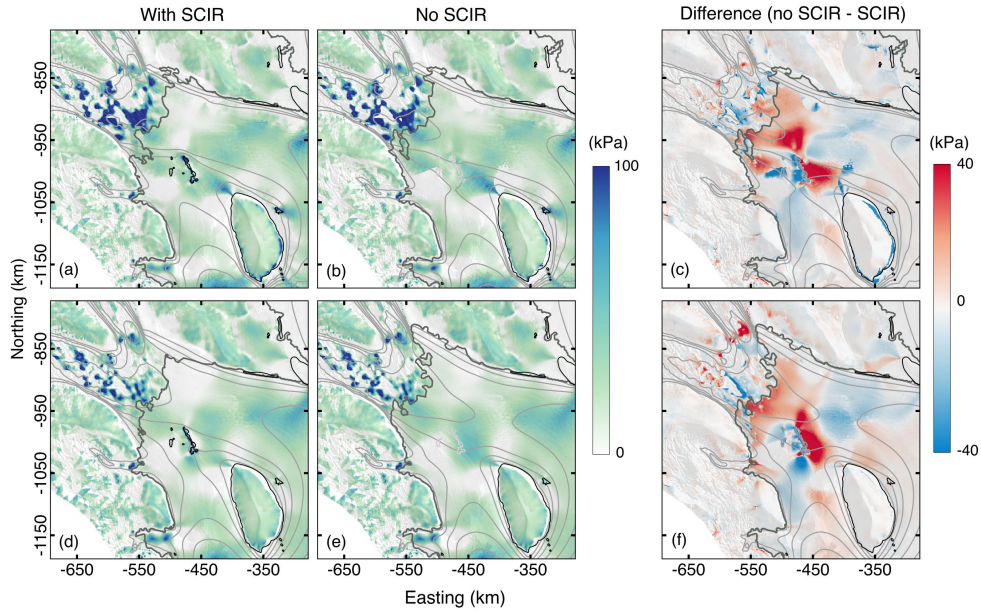


Figure 8: The transverse stress $+\bar{R}_{tt}$ (flow divergence) acting on the RIS and tributary ice streams with and without the SCIR. In (a-c), the model is initialised with \bar{B}_{invv} . In (d-f), the model is initialised with \bar{B}_u . In (c) and (f), positive (negative) values indicate an increase (decrease) in flow divergence when the SCIR are removed.

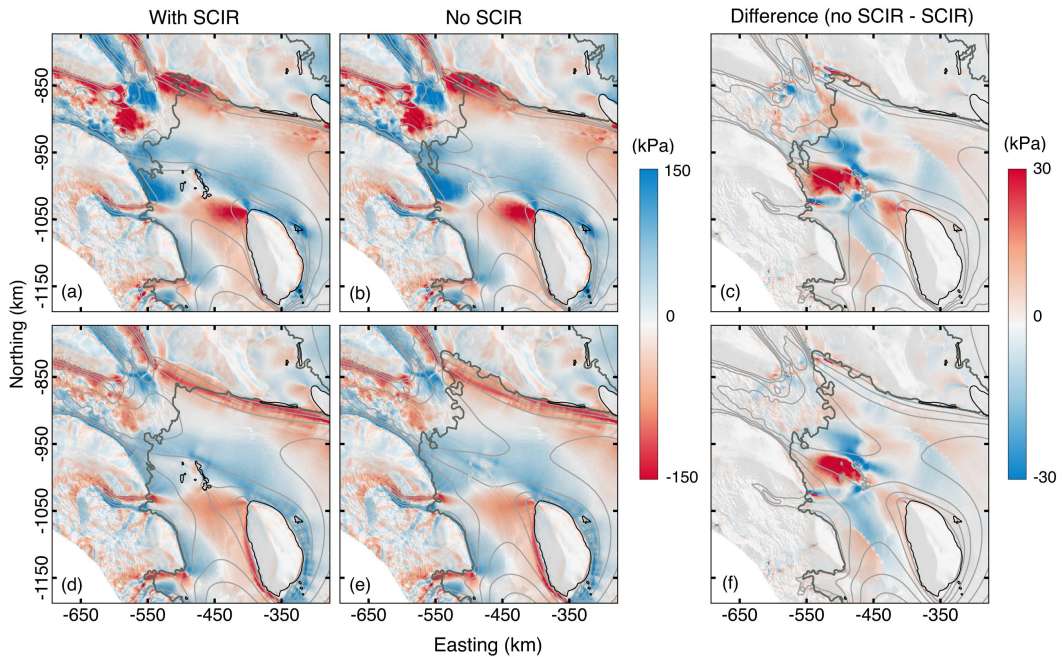


Figure 9: The lateral shear stress resisting RIS and tributary ice stream flow with and without the SCIR. Positive and negative \bar{R}_{lt} magnitudes denote shearing along glacier-left or glacier-right margins, respectively. Difference maps show the absolute difference in \bar{R}_{lt} . In (a-c), the simulation is initialised with \bar{B}_{invv} . In (d-f), the simulation is initialised with \bar{B}_u . In (c) and (f), a positive (negative) change indicates an increase (decrease) in \bar{R}_{lt} after removal of the SCIR.

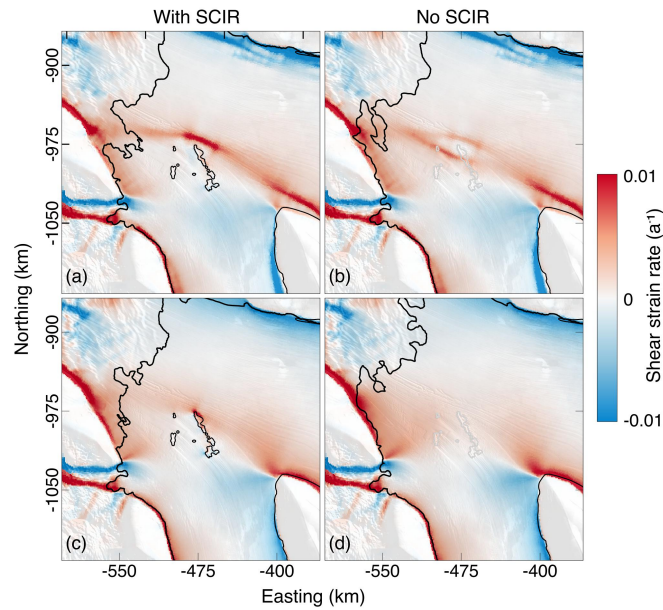


Figure 10: Model shear strain rates near the SCIR for (a) and (b) spatially variable ice properties (\bar{B}_{inv} model) versus (c) and (d) uniform ice properties (\bar{B}_u model). Grounding line positions are obtained from the reference and perturbed models.

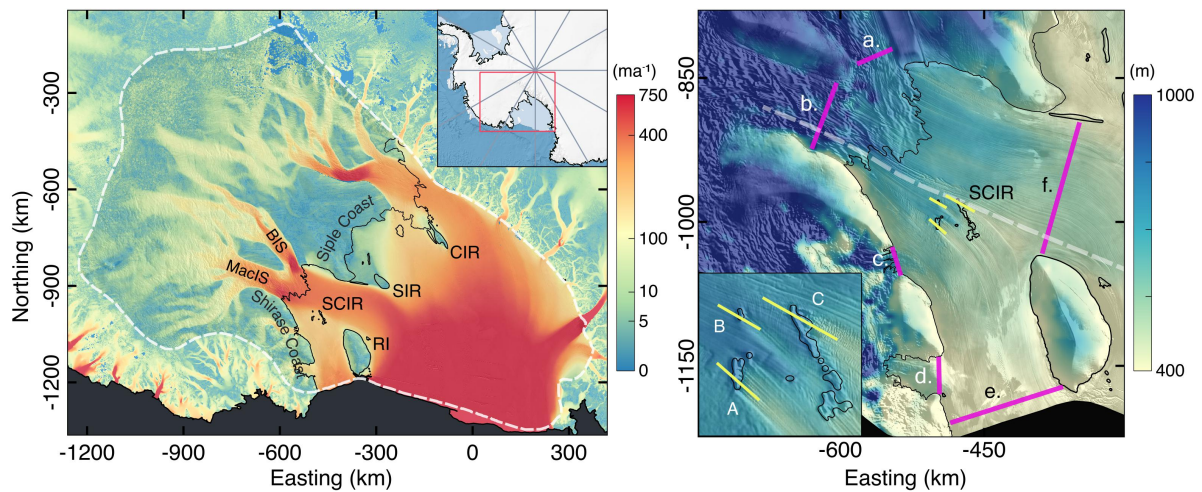


Figure 11: Pinning points in the RIS and the model domain boundary. In panel (a), large pinning points are labelled: SCIR = the Shirase Coast Ice Rumples, RI = Roosevelt Island, SIR = Steershead Ice Rise and CIR = Crary Ice Rise. The colour map of surface ice velocity magnitude is from the MEaSUREs velocity dataset (Rignot et al., 2011). The black line indicates the grounding zone (Bindschadler et al., 2011). Panel (b) shows the along-flow cross-sections intersecting the SCIR in Figs. 3 and 10 and the gates used for mass flux calculations in Table 3. The colour map of ice thickness is from the Bedmap2 compilation (Fretwell et al., 2013). In each figure from hereon, datasets are mapped with a Polar Stereographic Projection with a central meridian of 0° and a standard latitude of 71°S , and in most cases, overlaid onto the MODIS MOA (Haran et al., 2014).

References

- Anandakrishnan, S. and Alley, R. B. (1994). Ice Stream C, Antarctica, sticky spots detected by microearthquake monitoring. *Annals of Glaciology*, **20**, pp. 183–186. DOI: [10.3189/1994AoG20-1-183-186](https://doi.org/10.3189/1994AoG20-1-183-186).
- Bassis, J. N. and Ma, Y (2015). Evolution of basal crevasses links ice shelf stability to ocean forcing. *Earth and Planetary Science Letters*, **409**, pp. 203–211. DOI: [10.1016/j.epsl.2014.11.003](https://doi.org/10.1016/j.epsl.2014.11.003).
- Bindschadler, R, Choi, H, Wichlacz, A, Bingham, R, Bohlander, J, Brunt, K, Corr, H, Drews, R, Fricker, H, Hall, M, Hindmarsh, R, and Kohler, J (2011). Getting around Antarctica: new high-resolution mappings of the grounded and freely-floating boundaries of the Antarctic ice sheet created for the International Polar Year. *The Cryosphere*, **5** (3), pp. 569–588. DOI: [10.5194/tc-5-569-2011](https://doi.org/10.5194/tc-5-569-2011).
- Bindschadler, R. A and Scambos, T. A (1991). Satellite-Image-Derived Velocity Field of an Antarctic Ice Stream. *Science*, **252** (5003), pp. 242–246. DOI: [10.1126/science.252.5003.242](https://doi.org/10.1126/science.252.5003.242).
- Borstad, C., Mcgrath, D., and Pope, A. (2017). Fracture propagation and stability of ice shelves governed by ice shelf heterogeneity. *Geophysical Research Letters*, **44**, pp. 4186–4194. DOI: [10.1002/2017GL072648](https://doi.org/10.1002/2017GL072648).
- Brondeux, J., Gagliardini, O., Gillet-Chaulet, F., and Durand, G. (2017). Sensitivity of grounding line dynamics to the choice of the friction law. *Journal of Glaciology*, **63** (241), pp. 854–866. ISSN: 00221430. DOI: [10.1017/jog.2017.51](https://doi.org/10.1017/jog.2017.51).
- Budd, W. F., Keage, P. L., and Blundy, N. A. (1979). Empirical Studies of Ice Sliding. *Journal of Glaciology*, **23** (89), pp. 157–170. DOI: [10.1017/S0022143000029804](https://doi.org/10.1017/S0022143000029804).
- Duval, P and Castelnau, O (1995). Dynamic Recrystallization of Ice in Polar Ice Sheets. *Journal de Physique IV*, **111** (C3), p. 5. DOI: [10.1051/jp4:1995317](https://doi.org/10.1051/jp4:1995317).
- Fretwell, P. et al. (2013). Bedmap2: improved ice bed, surface and thickness datasets for Antarctica. *The Cryosphere*, **7** (1), pp. 375–393. DOI: [10.5194/tc-7-375-2013](https://doi.org/10.5194/tc-7-375-2013).
- Fürst, J. J., Durand, G., Gillet-Chaulet, F., Tavard, L., Rankl, M., Braun, M., and Gagliardini, O. (2016). The safety band of Antarctic ice shelves. *Nature Climate Change*, **6** (5), pp. 479–482. DOI: [10.1038/nclimate2912](https://doi.org/10.1038/nclimate2912).
- Gladstone, R. M., Lee, V., Vieli, A., and Payne, A. J. (2010). Grounding line migration in an adaptive mesh ice sheet model. *Journal of Geophysical Research*, **115** (F4), F04014. DOI: [10.1029/2009JF001615](https://doi.org/10.1029/2009JF001615).
- Gudmundsson, G. H., Paolo, F. S., Adusumilli, S., and Fricker, H. A. (2019). Instantaneous Antarctic ice sheet mass loss driven by thinning ice shelves. *Geophysical Research Letters*, **46** (23), pp. 13903–13909. ISSN: 0094-8276. DOI: [10.1029/2019GL085027](https://doi.org/10.1029/2019GL085027).
- Haran, T., Bohlander, J., Scambos, T., Painter, T., and Fahnestock, M. (2014). MODIS Mosaic of Antarctica 2008-2009 (MOA2009) Image Map. DOI: [10.7265/N5KP8037](https://doi.org/10.7265/N5KP8037).
- Haseloff, M. and Sergienko, O. V. (2018). The effect of buttressing on grounding line dynamics. *Journal of Glaciology*, **64** (245), pp. 417–431. DOI: [10.1017/jog.2018.30](https://doi.org/10.1017/jog.2018.30).
- Jordan, T. M., Schroeder, D. M., Elsworth, C. W., and Siegfried, M. R. (2020). Estimation of ice fabric within Whillans Ice Stream using polarimetric phase-sensitive radar sounding. *Annals of Glaciology*, **61** (81), pp. 74–83. ISSN: 02603055. DOI: [10.1017/aog.2020.6](https://doi.org/10.1017/aog.2020.6).
- Joughin, I., MacAyeal, D. R., and Tulaczyk, S. (2004). Basal shear stress of the Ross ice streams from control method inversions. *Journal of Geophysical Research: Solid Earth*, **109** (B9), B09405. DOI: [10.1029/2003JB002960](https://doi.org/10.1029/2003JB002960).

- Joughin, I., Smith, B. E., and Schoof, C. G. (2019). Regularized Coulomb Friction Laws for Ice Sheet Sliding: Application to Pine Island Glacier, Antarctica. *Geophysical Research Letters*, **46** (9), pp. 4764–4771. ISSN: 0094-8276. DOI: [10.1029/2019GL082526](https://doi.org/10.1029/2019GL082526).
- Lai, C.-Y., Kingslake, J., Wearing, M., Po-Hsuan Chen Cameron, Gentine, P., Li, H., Spergel, J., and Wessem, J. M. van (2020). Vulnerability of Antarctica's ice shelves to meltwater-driven fracture. *Nature*, **584**, pp. 574–578. DOI: [10.1038/s41586-020-2627-8](https://doi.org/10.1038/s41586-020-2627-8).
- Luthra, T., Anandakrishnan, S., Winberry, J. P., Alley, R. B., and Holschuh, N. (2016). Basal characteristics of the main sticky spot on the ice plain of Whillans Ice Stream, Antarctica. *Earth and Planetary Science Letters*, **440**, pp. 12–19. DOI: [10.1016/J.EPSL.2016.01.035](https://doi.org/10.1016/J.EPSL.2016.01.035).
- Lutz, F., Eccles, J., Prior, D. J., Craw, L., Fan, S., Hulbe, C., Forbes, M., Still, H., Pyne, A., and Mandeno, D. (2020). Constraining Ice Shelf Anisotropy Using Shear Wave Splitting Measurements from Active-Source Borehole Seismics. *Journal of Geophysical Research: Earth Surface*, **125** (9). ISSN: 2169-9003. DOI: [10.1029/2020JF005707](https://doi.org/10.1029/2020JF005707).
- Nias, I. J., Cornford, S. L., and Payne, A. J. (2016). Contrasting the modelled sensitivity of the Amundsen Sea Embayment ice streams. *Journal of Glaciology*, **62** (233), pp. 552–562. DOI: [10.1017/jog.2016.40](https://doi.org/10.1017/jog.2016.40).
- Pegler, S. S. (2018). Marine ice sheet dynamics: The impacts of ice-shelf buttressing. *Journal of Fluid Mechanics*, **857**, pp. 605–647. DOI: [10.1017/jfm.2018.741](https://doi.org/10.1017/jfm.2018.741).
- Rignot, E., Mouginot, J., and Scheuchl, B. (2011). MEaSURES InSAR-Based Antarctica Ice Velocity Map. DOI: [10.5067/measures/cryosphere/nsidc-0484.001](https://doi.org/10.5067/measures/cryosphere/nsidc-0484.001).
- Sanderson, T. J. O. (1979). Equilibrium Profile of Ice Shelves. *Journal of Glaciology*, **22** (88), pp. 435–460. DOI: [10.3189/s0022143000014453](https://doi.org/10.3189/s0022143000014453).
- Schoof, C. (2007). Ice sheet grounding line dynamics: Steady states, stability, and hysteresis. *Journal of Geophysical Research*, **112** (F3), F03S28. DOI: [10.1029/2006JF000664](https://doi.org/10.1029/2006JF000664).
- Sergienko, O. V., Bindschadler, R. A., Vornberger, P. L., and MacAyeal, D. R. (2008). Ice stream basal conditions from block-wise surface data inversion and simple regression models of ice stream flow: Application to Bindschadler Ice Stream. *Journal of Geophysical Research*, **113** (F4), F04010. DOI: [10.1029/2008JF001004](https://doi.org/10.1029/2008JF001004).
- Seroussi, H., Morlighem, M., Larour, E., Rignot, E., and Khazendar, A. (2014). Hydrostatic grounding line parameterization in ice sheet models. *The Cryosphere*, **8**, pp. 2075–2087. DOI: [10.5194/tc-8-2075-2014](https://doi.org/10.5194/tc-8-2075-2014).
- Seroussi, H. and Morlighem, M. (2018). Representation of basal melting at the grounding line in ice flow models. *The Cryosphere*, **12**, pp. 3085–3096. DOI: [10.5194/tc-12-3085-2018](https://doi.org/10.5194/tc-12-3085-2018).
- Stephenson, S. and Bindschadler, R. (1990). Is Ice-Stream Evolution Revealed By Satellite Imagery? *Annals of Glaciology*, **14**, pp. 273–277. DOI: [10.3189/S0260305500008740](https://doi.org/10.3189/S0260305500008740).
- Still, H., Campbell, A., and Hulbe, C. (2019). Mechanical analysis of pinning points in the Ross Ice Shelf, Antarctica. *Annals of Glaciology*, **60** (78), pp. 32–41. DOI: [10.1017/aog.2018.31](https://doi.org/10.1017/aog.2018.31).
- Tsai, V. C., Stewart, A. L., and Thompson, A. F. (2015). Marine ice-sheet profiles and stability under Coulomb basal conditions. *Journal of Glaciology*, **61** (226), pp. 205–215. ISSN: 00221430. DOI: [10.3189/2015JogG14J221](https://doi.org/10.3189/2015JogG14J221).
- Weertman, J. (1974). Stability of the Junction of an Ice Sheet and an Ice Shelf. *Journal of Glaciology*, **13** (67), pp. 3–11. DOI: [10.3189/S0022143000023327](https://doi.org/10.3189/S0022143000023327).